Heteroatom-Doped [4]Triangulene: Facile Synthesis and Two-Dimensional On-Surface Self-Assemblies

Cheng Chen,[†,▽] Jiayi Lu,[‡,▽] Yang Lv,[†] Yuyi Yan,[‡] Qiang Sun,*[,‡] Akimitsu Narita,[§] Klaus Müllen,*[,§,#] and Xiao-Ye Wang*[,†]

[†]State Key Laboratory of Elemento-Organic Chemistry, College of Chemistry, Nankai University, Tianjin 300071, China

[‡]Materials Genome Institute, Shanghai University, 200444 Shanghai, China

[§]Max Planck Institute for Polymer Research, 55128 Mainz, Germany

[#]Department of Chemistry, Johannes Gutenberg University Mainz, Duesbergweg 10-14, 55128 Mainz, Germany

ABSTRACT: Synthesis of nanographenes (NGs) with structural precision has attracted enormous interest in organic chemistry and materials science. However, their ordered two-dimensional (2D) self-assembled structures on surfaces, which are of great importance for the future nanotechnologies, remain challenging. In this work, embedding heteroatoms (oxygen-boron-oxygen) into the zigzag edges of NGs is proven as a useful strategy to afford ordered 2D self-assemblies based upon intermolecular hydrogen bonding. We have thus synthesized OBO-doped [4]triangulenes, whose planar geometry is revealed by single-crystal X-ray diffraction. Their photophysical and electrochemical properties show significant differences from those of pristine [4]triangulene. Self-assembly on metal surfaces is explored by scanning tunneling microscopy (STM) associated with the minimum spanning tree (MST) analysis. Highly ordered 2D superstructures can be demonstrated and the packing modes depend sensitively upon the substrate.

Nanographenes (NGs), namely nanoscale graphene fragments, have been considered as next-generation semiconductors due to their potential in, for example, optoelectronics, bio-imaging, and energy storage.[1-5] Bottom-up fabrication of NGs is crucial for controlling their structures at the atomic level and precisely tuning their functions. During the past years, a large number of structurally well-defined NGs with various sizes and topological features have been synthesized in solution and on metal surfaces.[6-17] Furthermore, incorporation of heteroatoms has further expanded the possibilities of generating novel structures with desirable properties.[18-23]

On the other hand, steering molecular assembly to form ordered two-dimensional (2D) networks has attracted much attention due to the superiority of 2D materials for optoelectronic applications.[24-29] Many efforts have been devoted to constructing molecular 2D architectures on metal surfaces by adjusting intermolecular and molecule–substrate interactions.[30-37] Nevertheless, it remains a significant challenge for NGs to form 2D self-assembled structures owing to the lack of lateral interactions among the large NGs.[1] So far, only very few NG-based 2D assemblies have been reported, mainly driven by intermolecular $\pi\cdots\pi$ interactions (in the case of curved NGs)[36] and templating effects of the surface.[38] Attractive intermolecular forces driving the formation of 2D networks based on planar NGs have been less explored, although they have played an important role in the design of various 2D organic nanostructures.[39-41]

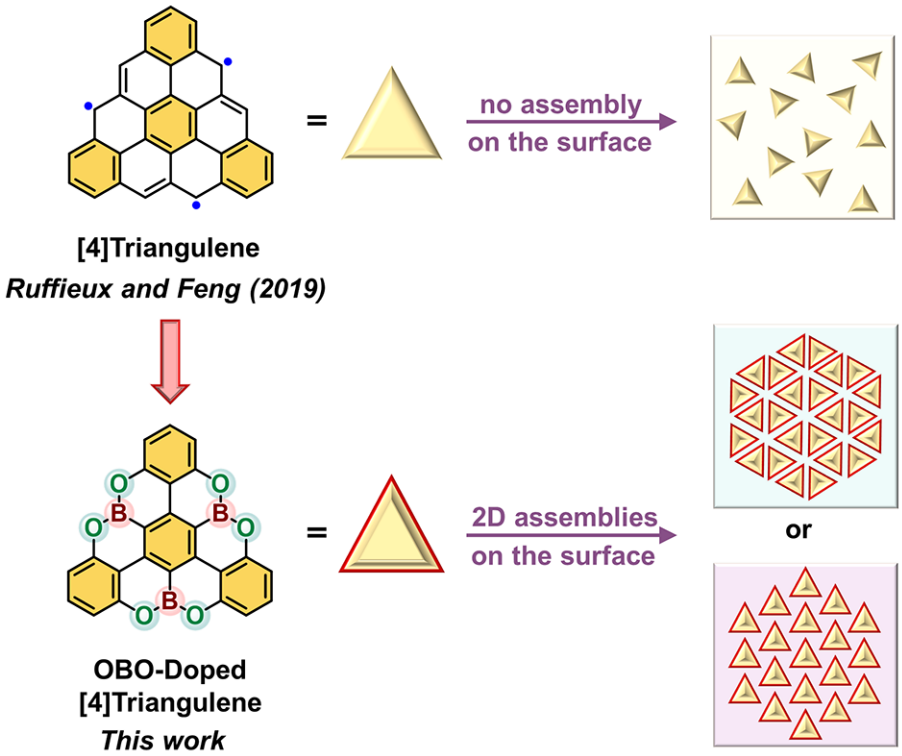

Figure 1. Chemical structures of [4]triangulene and the OBO-doped [4]triangulene reported in this work, as well as the schematic representations of their on-surface self-assembled behaviors.

Herein, embedding heteroatoms into the zigzag edges of NGs is shown to furnish highly ordered 2D nanoarchitectures of NGs, without the need of attaching pendent attracting substituents (Figure 1). A variety of zigzag-edged triangular NGs, namely triangulenes, have been synthesized on metal surfaces recently, mainly displaying random distribution patterns on the substrate.[42] Toward extended 2D assemblies, oxygen-boron-oxygen (OBO) segments are incorporated into the three zigzag edges of [4]triangulene, leading to OBO-doped [4]triangulenes with high ambient stability. Importantly, highly ordered 2D self-assemblies driven by intermolecular C–H···O hydrogen bonds are observed on different substrates,[43,44] and an interesting substrate-dependent assembly behavior is observed, thus demonstrating the great potential of OBO-doped triangulenes for constructing 2D functional materials.

Scheme 1. Synthetic route to OBO-doped NGs 1a and 1b.

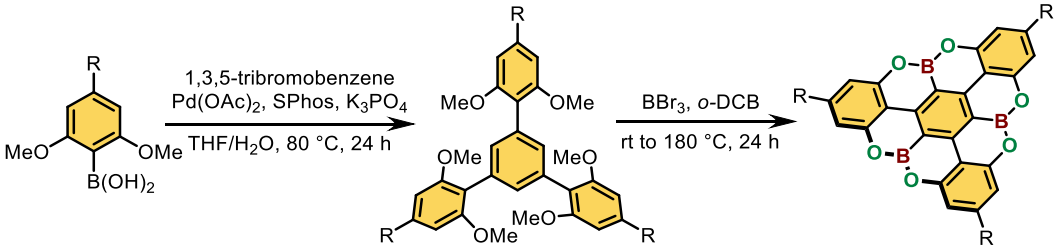

The synthetic route to OBO-doped [4]triangulenes **1a** and **1b** is depicted in Scheme 1.[45] The corresponding precursors **3a** and **3b** were synthesized through a Suzuki coupling reaction of 1,3,5-tribromobenzene and two aryl boronic acids (**2a** and **2b**) in 92% and 91% yields, respectively. Boron atoms were then incorporated into the skeleton by the tandem demethylation-electrophilic borylation reaction,[46,47] giving air-stable **1a** and **1b** as white solids in 82% and 95% yields, respectively. Compound **1b** was well soluble in common organic solvents and characterized by ^{1}H and ^{13}C NMR spectroscopies as well as high-resolution mass spectrometry (HRMS), whereas compound **1a** was only characterized by ^{1}H NMR spectroscopy and HRMS due to its poor solubility.

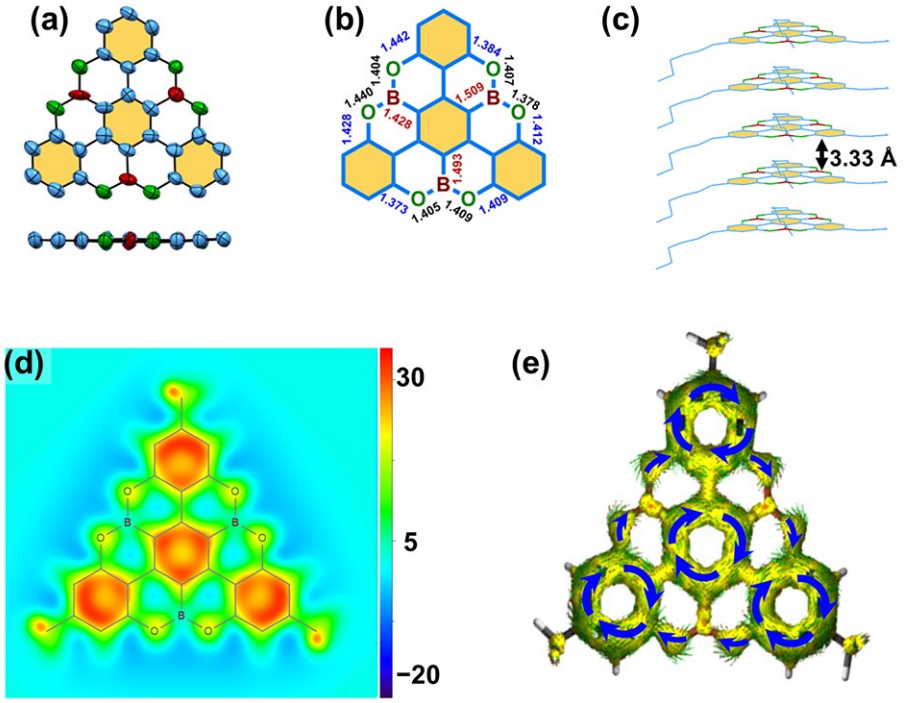

Figure 2. (a) Single-crystal X-ray structure of **1b** (top and side view). Thermal ellipsoids are shown at 50% probability. Alkyl chains and hydrogen atoms are omitted for clarity. (b) Selected bond lengths and (c) packing diagrams of **1b**. (d) Calculated 2D ICSS(1)$_{zz}$ maps and (e) ACID plots of **1b** at 1 Å above the XY plane. Alkyl chains are replaced by methyl groups for simplicity during the calculations.

Single crystal of **1b** was successfully obtained, allowing or X-ray structural analysis. Compound **1b** exhibits a fully planar π-conjugated framework, indicating the minimum effect of OBO units on the planarity of the molecule (Figure 2a). In the C$_4$BO rings, the B–O bond lengths (1.38–1.44 Å) are similar to the common B–O single bonds, whereas the C–O bonds (1.37–1.44 Å) are slightly longer, as compared with the previously reported oxaborines (1.37–1.39 Å) (Figure 2b).[46] It is noteworthy that the C–B bonds (1.43–1.51 Å) are significantly shorter than the classic C–B single bonds in triphenylborane (1.57–1.59 Å) as well as those in oxaborines (1.52–1.54 Å), indicating the effective π-delocalization from the central benzene ring to the empty *p*-orbital of the boron center. Interestingly, compound **1b** displays a column stacking structure with a short π-π distance of only 3.33 Å (Figure 2c). The calculated isotropic chemical shielding surface (ICSS) maps and the anisotropy of the induced current density (ACID) plots reveal that the benzene rings are aromatic while the C$_4$BO rings are non-aromatic (Figure 2d and e).

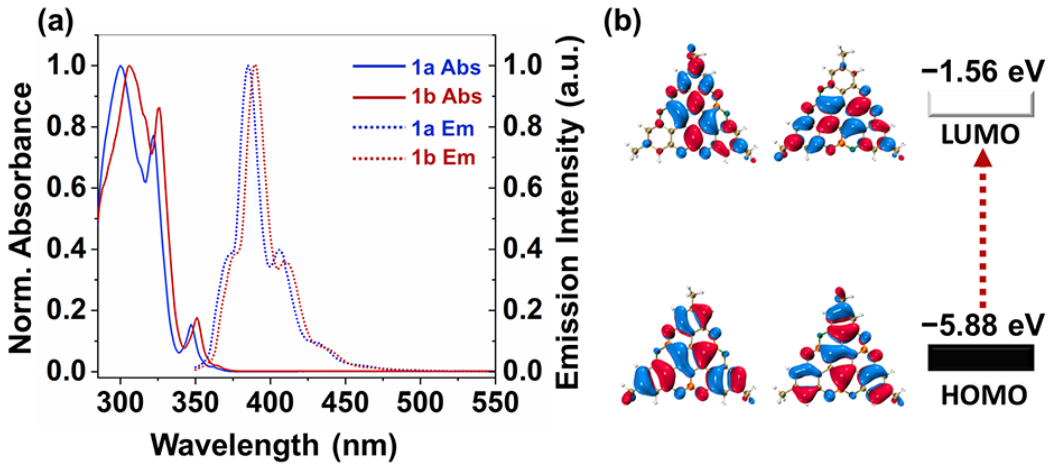

Figure 3. (a) Normalized UV-vis absorption and emission spectra of **1a** (blue) and **1b** (red) in toluene solutions. (b) TDDFT-calculated degenerated frontier molecular orbitals and the energy diagram of **1b**. Alkyl chains are replaced by methyl groups for simplicity during the calculations.

UV-vis absorption and fluorescence spectra of **1a** and **1b** were recorded in dilute toluene solutions (Figure 3a). Two compounds exhibit similar absorption features in the UV region with three major electronic absorption bands. The lowest energy band for **1a** peaks at 347 nm, whereas **1b** shows a slightly red-shifted absorption maximum at 351 nm. Time-dependent density functional theory (TDDFT) calculations reveal that the low-energy absorption band is assignable to the HOMO→LUMO transition, and HOMO and LUMO are delocalized over the whole skeleton (Figure 3b and Table S3). Furthermore, compounds **1a** and **1b** display similar emission spectra peaking at 385 and 390 nm with absolute fluorescence quantum yields of 57% and 58%, respectively.

The electrochemical properties of **1b** were studied by cyclic voltammetry (CV) and differential pulse voltammetry (DPV) measurements, whereas the same characterization for **1a** was hindered by its low solubility (Figure S1). According to the DPV results, the HOMO and LUMO energy levels of compound **1b** are estimated as −5.95 and −2.69 eV, respectively. The electrochemical HOMO-LUMO gap of **1b** is thus determined as 3.26 eV, which is in good agreement with the optical gap that is deduced from the absorption onset (3.28 eV).

Previous studies have demonstrated that NGs with OBO edges tend to form ordered superstructures on metal surfaces via the intermolecular C–H…O hydrogen bonds.[43,44] Hence, the self-assembled behavior of **1a** on metal surfaces was investigated. A sub-monolayer of the molecules was deposited on different substrates under ultra-high vacuum (UHV) conditions, yielding self-assembled structures according to molecule-resolved scanning tunneling microscopy (STM) images. The less regular 2D assemblies of **1a** are observed on Au(111) surface, showing two different phases denoted as phase I and phase II (Figure 4a and b). High-resolution STM images indicate that phase I is composed of two specific structural motifs, named α and γ, whereas phase II consists of binding motifs β and γ (Figure 4e, f; the binding modes are shown in Figure i). In contrast, **1a** exhibits a highly ordered close-packed structure on Ag(111) surface and a porous structure (pore-to-pore distance of ~1.95 nm) on Cu(111) surface with consistent structural motifs β and γ, respectively (Figure 4c,d,g,h).

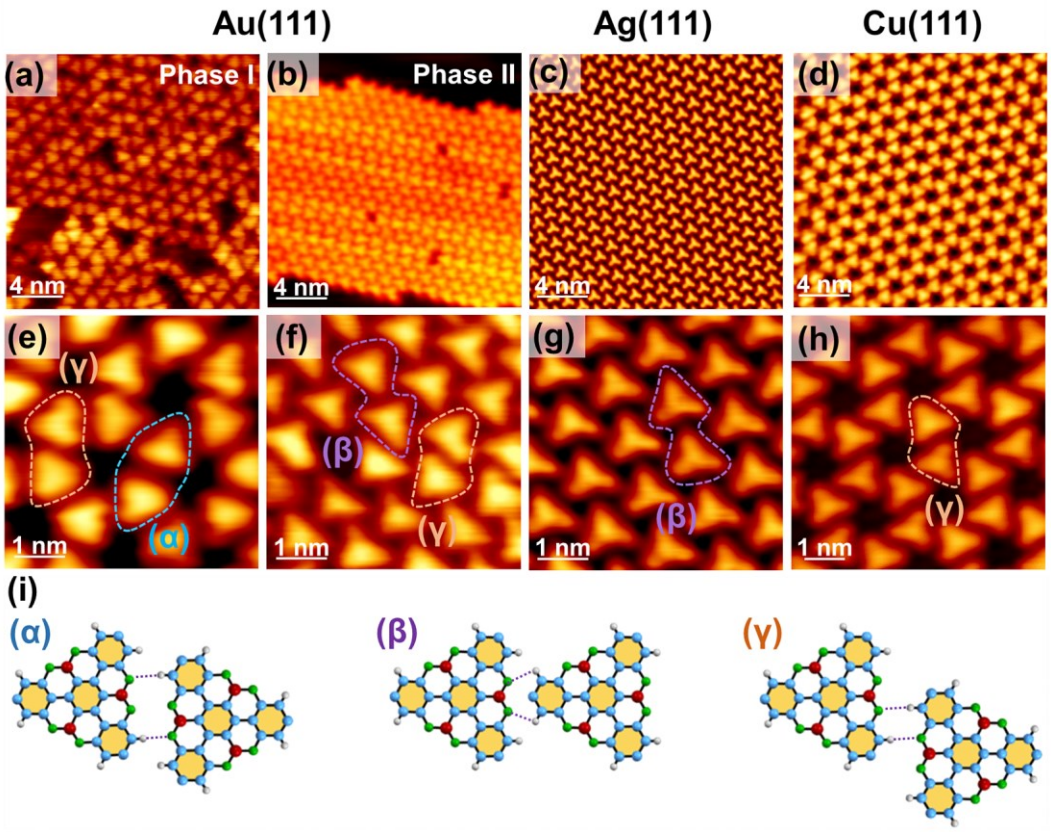

Figure 4. STM images of the self-assembled structures of **1a** on the (a, b) Au(111), (c) Ag(111) and (d) Cu(111) substrates. Enlarged images of the self-assembled structures on the (e, f) Au(111), (g) Ag(111) and (h) Cu(111) substrates. (i) Three characteristic structural motifs of the **1a** dimer (α, β, γ), with the hydrogen bonds indicated by dashed lines. In e–h, the dimeric binding motifs are marked with dashed contours. Tunneling parameters are I_t = 150 pA, V_b = −1.0 V for (a); I_t = 80 pA, V_b = −1.0 V for (b); I_t = 500 pA, V_b = −1.0 V for (c); I_t = 50 pA, V_b = −1.5 V for (d); I_t = 150 pA, V_b = −0.4 V for (e); I_t = 110 pA, V_b = −1.0 V for (f); I_t = 50 pA, V_b = −1.0 V for (g); I_t = 150 pA, V_b = −2.0 V for (h).

In order to understand the unique assembled behavior, DFT calculations on the dimeric binding motifs and the assembly structures were performed (Figure S7). The three motifs exhibit similar binding energies of −0.163 eV for α, −0.111 eV for β, and −0.168 eV for γ, which verifies the existence of different assembly structures on Au(111) surface. Moreover, the extended arrangement built from motif α shows a higher relative energy (defined as 0 eV) compared with that of motifs β (−0.267 eV) and γ (−0.089 eV). This can explain the disappearance of motif α on Ag and Cu substrates. Furthermore, the relative stronger interactions between **1a** and Ag/Cu substrate may also facilitate the formation of highly ordered 2D self-assemblies.[27]

We then performed the minimum spanning tree (MST) analysis of the STM image of **1a** on Ag(111) surface to quantify the degrees of disorder of the 2D self-assembled structures (Figure 5a).[48-50] Based on the MST image, a Voronoi tessellation can be constructed, representing molecules with various highly ordered hexagonal cells (Figure 5b). Besides, the mean normalized distance (μ) of MST image edges (green lines) is calculated as ~1.045 with a standard deviation (σ) of ~0.021 (Figure 5c). According to the characteristic $\mu-\sigma$ plots of different lattices, the 2D structure of **1a** on Ag(111) surface is assigned as the triangular lattice To systematically investigate the 2D architectures on different surfaces, the MST analysis of large-scale STM images is also conducted, revealing that the self-assembled modes of phase I on Au(111) surface and on Cu(111) surface are assigned as the honeycomb lattice, whereas the assembly of phase II on Au(111) surface is regarded as the triangular lattice (Figure 5d). In addition, the superstructures of **1a** show higher values of standard deviation on Au(111) surface (σ = 0.116 for phase I and 0.084

for phase II) than those on Ag(111) surface (σ = 0.030) and on Cu(111) surface (σ = 0.040), which is in accordance with the observations of more motifs on Au(111) surface.

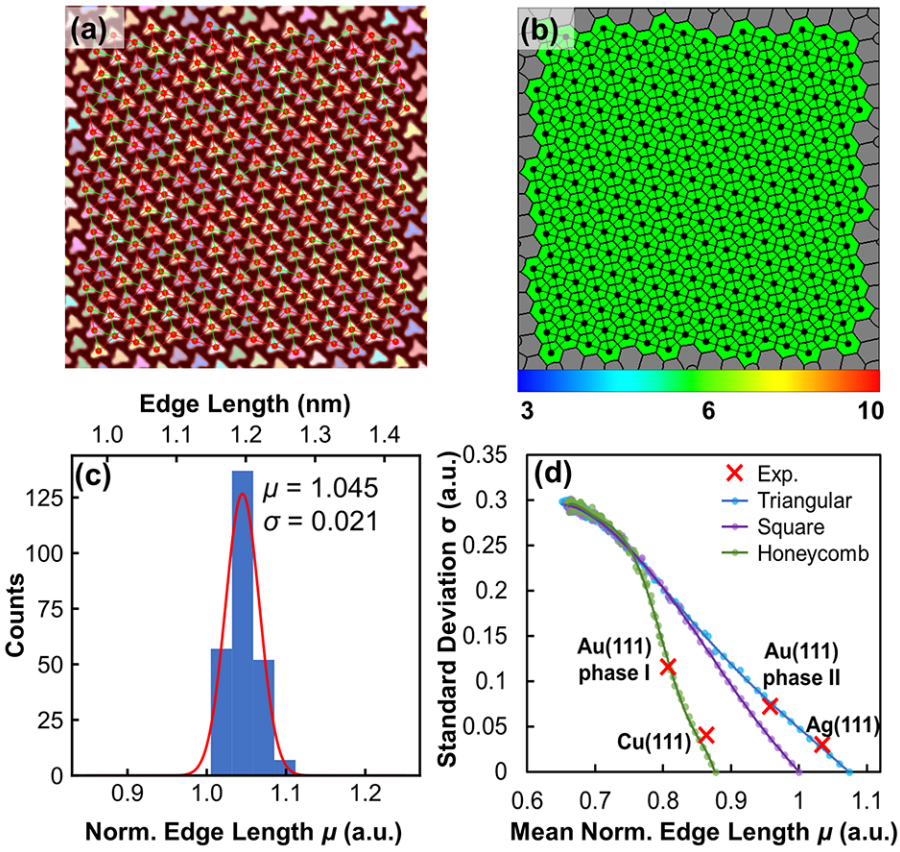

Figure 5. (a) MST analysis of **1a** on Ag(111), overlaid with an arbitrary color scheme used for identifying each molecule (the corresponding STM image is illustrated in Figure 4c). The mass center of each molecule is selected as nodes; the red edges represent the distance between neighboring nodes; the green edges represent the shortest distance of the disjoint red lines that link all of the nodes. (b) Voronoi tessellation of the MST image. Color coded by the number of edges of each cell. (c) Histogram of the MST's edge length. (d) μ versus σ deviation of the MST's edge length. The dots fitted as solid lines show the distortion trajectory from the (μ, σ) plots of the ideal triangular, square and honeycomb lattices (at σ = 0) to a random distribution of nodes. The red crosses represent the μ–σ values of experimentally observed self-assembled structures.

In summary, we have synthesized the unprecedented air-stable OBO-doped [4]triangulenes **1a** and **1b**. The structure of **1b** is unambiguously determined by single-crystal X-ray analysis. The photophysical and electrochemical properties have been investigated in conjunction with theoretical calculations. Moreover, highly ordered 2D self-assemblies of **1a** are observed on metal surfaces, driven by intermolecular C–H···O hydrogen bonding interactions. Furthermore, different substrates exert a significant influence on the self-assembled structures, leading to a uniform triangular lattice on Ag(111) surface and a honeycomb lattice on Cu(111) surface. This work provides a potential heteroatom-doping strategy for realizing 2D self-assembly of NGs, which could stimulate the development of novel NG-based 2D materials for future nanotechnological applications.

ASSOCIATED CONTENT

The Supporting Information is available as a PDF file.

Accession Code

CCDC 2196043 contains the supplementary crystallographic data for this paper. These data can be obtained free of charge via www.ccdc.cam.ac.uk/data_request/cif, or by emailing data_request@ccdc.cam.ac.uk, or by contacting The Cambridge Crystallographic Data Centre, 12 Union Road, Cambridge CB2 1EZ, U.K.; fax: +44 1223 336033.

AUTHOR INFORMATION

Corresponding Author

*Email: qiangsun@shu.edu.cn
*Email: muellen@mpip-mainz.mpg.de
*Email: xiaoye.wang@nankai.edu.cn

Author Contributions

▽These authors contributed equally.

Notes

The authors declare no competing financial interest.

ACKNOWLEDGMENT

We are grateful to the financial support from the National Natural Science Foundation of China (Nos. 21901128 and 22071120), the National Key R&D Program of China (2020YFA0711500), the Fundamental Research Funds for the Central Universities, and the Max Planck Society. K.M. acknowledges a fellowship from Gutenberg Research College, Johannes Gutenberg University Mainz. The authors cordially thank Dr. Dieter Schollmeyer (Department of Chemistry, Johannes Gutenberg University Mainz) for single-crystal X-ray structural analysis.

REFERENCES

(1) Wu, J.; Pisula, W.; Müllen, K.; Graphenes as potential material for electronics. *Chem. Rev.* **2007,** *107*, 718-747.
(2) Narita, A.; Wang, X.-Y.; Feng, X.; Müllen, K.; New advances in nanographene chemistry. *Chem. Soc. Rev.* **2015,** *44*, 6616-6643.
(3) Liu, J.; Feng, X.; Synthetic tailoring of graphene nanostructures with zigzag-edged topologies: Progress and perspectives. *Angew. Chem. Int. Ed.* **2020,** *59*, 23386-23401.
(4) Gu, Y.; Qiu, Z.; Müllen, K.; Nanographenes and graphene nanoribbons as multitalents of present and future materials science. *J. Am. Chem. Soc.* **2022,** *144*, 11499-11524.
(5) Wang, X.-Y.; Yao, X.; Müllen, K.; Polycyclic aromatic hydrocarbons in the graphene era. *Sci. China Chem.* **2019,** *62*, 1099-1144.
(6) Wang, X.-Y.; Narita, A.; Müllen, K.; Precision synthesis versus bulk-scale fabrication of graphenes. *Nat. Rev. Chem.* **2018,** *2*, 0100.
(7) Xiang, F.; Maisel, S.; Beniwal, S.; Akhmetov, V.; Ruppenstein, C.; Devarajulu, M.; Dörr, A.; Papaianina, O.; Görling, A.; Amsharov, K. Y.; Maier, S.; Planar π-extended cycloparaphenylenes featuring an all-armchair edge topology. *Nat. Chem.* **2022**, DOI: 10.1038/s41557-41022-00968-41553.
(8) Zeng, W.; Wu, J.; Open-Shell Graphene Fragments. *Chem* **2021,** *7*, 358-386.

(9) Mishra, S.; Catarina, G.; Wu, F.; Ortiz, R.; Jacob, D.; Eimre, K.; Ma, J.; Pignedoli, C. A.; Feng, X.; Ruffieux, P.; Fernández-Rossier, J.; Fasel, R.; Observation of fractional edge excitations in nanographene spin chains. *Nature* **2021,** *598*, 287-292.
(10) Wang, X.; Ma, J.; Zheng, W.; Osella, S.; Arisnabarreta, N.; Droste, J.; Serra, G.; Ivasenko, O.; Lucotti, A.; Beljonne, D.; Bonn, M.; Liu, X.; Hansen, M. R.; Tommasini, M.; De Feyter, S.; Liu, J.; Wang, H. I.; Feng, X.; Cove-edged graphene nanoribbons with incorporation of periodic zigzag-edge segments. *J. Am. Chem. Soc.* **2022,** *144*, 228-235.
(11) Song, S.; Su, J.; Telychko, M.; Li, J.; Li, G.; Li, Y.; Su, C.; Wu, J.; Lu, J.; On-surface synthesis of graphene nanostructures with π-magnetism. *Chem. Soc. Rev.* **2021,** *50*, 3238-3262.
(12) Gu, Y.; Vega-Mayoral, V.; Garcia-Orrit, S.; Schollmeyer, D.; Narita, A.; Cabanillas-González, J.; Qiu, Z.; Müllen, K.; Cove-edged hexa-*peri*-hexabenzo-bis-*peri*-octacene: Molecular conformations and amplified spontaneous emission. *Angew. Chem. Int. Ed.* **2022,** *61*, e202201088.
(13) Fei, Y.; Liu, J.; Synthesis of Defective Nanographenes Containing Joined Pentagons and Heptagons. *Adv. Sci.* **2022**, e2201000.
(14) Fei, Y.; Fu, Y.; Bai, X.; Du, L.; Li, Z.; Komber, H.; Low, K. H.; Zhou, S.; Phillips, D. L.; Feng, X.; Liu, J.; Defective Nanographenes Containing Seven-Five-Seven (7-5-7)-Membered Rings. *J. Am. Chem. Soc.* **2021,** *143*, 2353-2360.
(15) Liu, P.; Chen, X.-Y.; Cao, J.; Ruppenthal, L.; Gottfried, J. M.; Müllen, K.; Wang, X.-Y.; Revisiting acepleiadylene: Two-step synthesis and π-extension toward nonbenzenoid nanographene. *J. Am. Chem. Soc.* **2021,** *143*, 5314-5318.
(16) Wang, Y.; Huang, Y.; Huang, T.; Zhang, J.; Luo, T.; Ni, Y.; Li, B.; Xie, S.; Zeng, Z.; Perylene-Based Linear Nonalternant Nanoribbons with Bright Emission and Ambipolar Redox Behavior. *Angew. Chem. Int. Ed.* **2022,** *61*, e202200855.
(17) Chai, L.; Ju, Y. Y.; Xing, J. F.; Ma, X. H.; Zhao, X. J.; Tan, Y.-Z.; Nanographene metallaprisms: Structure, stimulated transformation, and emission enhancement. *Angew. Chem. Int. Ed.* **2022,** *61*, e202210268.
(18) Borissov, A.; Maurya, Y. K.; Moshniaha, L.; Wong, W. S.; Zyla-Karwowska, M.; Stepien, M.; Recent Advances in Heterocyclic Nanographenes and Other Polycyclic Heteroaromatic Compounds. *Chem. Rev.* **2022,** *122*, 565-788.
(19) Yuan, L.; Guo, J.; Yang, Y.; Ye, K.; Dou, C.; Wang, Y.; A $C_{54}B_2$ polycyclic π-system with bilayer assembly and multi-redox activity. *CCS Chem.* **2022**, DOI: 10.31635/ccschem.31022.202101738.
(20) Zhang, H.; Lu, J.; Zhang, Y.; Gao, L.; Zhao, X.-J.; Tan, Y.-Z.; Cai, J.; Magnetism engineering of nanographene: an enrichment strategy by co-depositing diverse precursors on Au(111). *Chin. Chem. Lett.* **2022**, DOI: 10.1016/j.cclet.2022.1004.1048.
(21) Zhao, M.; Miao, Q.; Design, synthesis and hydrogen bonding of B_3N_6-[4]triangulene. *Angew. Chem. Int. Ed.* **2021,** *60*, 21289-21294.
(22) Wang, X.-Y.; Yao, X.; Narita, A.; Müllen, K.; Heteroatom-doped nanographenes with structural precision. *Acc. Chem. Res.* **2019,** *52*, 2491-2505.
(23) Stępień, M.; Gońka, E.; Żyła, M.; Sprutta, N.; Heterocyclic nanographenes and other polycyclic heteroaromatic compounds: Synthetic routes, properties, and applications. *Chem. Rev.* **2017,** *117*, 3479-3716.
(24) Xing, L.; Peng, Z.; Li, W.; Wu, K.; On controllability and applicability of surface molecular self-assemblies. *Acc. Chem. Res.* **2019,** *52*, 1048-1058.
(25) Yang, F.; Cheng, S.; Zhang, X.; Ren, X.; Li, R.; Dong, H.; Hu, W.; 2D organic materials for optoelectronic applications. *Adv. Mater.* **2018,** *30*, 1702415.
(26) Goronzy, D. P.; Ebrahimi, M.; Rosei, F.; Arramel; Fang, Y.; De Feyter, S.; Tait, S. L.; Wang, C.; Beton, P. H.; Wee, A. T. S.; Weiss, P. S.; Perepichka, D. F.; Supramolecular assemblies on surfaces: Nanopatterning, functionality, and reactivity. *ACS Nano* **2018,** *12*, 7445-7481.

(27) Tian, T.; Shih, C.-J.; Molecular epitaxy on two-dimensional materials: The interplay between interactions. *Ind. Eng. Chem. Res.* **2017,** *56*, 10552-10581.
(28) Otero, R.; Gallego, J. M.; Vázquez de Parga, A. L.; Martín, N.; Miranda, R.; Molecular self-assembly at solid surfaces. *Adv. Mater.* **2011,** *23*, 5148-5176.
(29) Fa, S.; Kakuta, T.; Yamagishi, T.-a.; Ogoshi, T.; One-, two-, and three-dimensional supramolecular assemblies based on tubular and regular polygonal structures of pillar[n]arenes. *CCS Chem.* **2019,** *1*, 50-63.
(30) Pfeiffer, C. R.; Pearce, N.; Champness, N. R.; Complexity of two-dimensional self-assembled arrays at surfaces. *Chem. Commun.* **2017,** *53*, 11528-11539.
(31) Mali, K. S.; Pearce, N.; De Feyter, S.; Champness, N. R.; Frontiers of supramolecular chemistry at solid surfaces. *Chem. Soc. Rev.* **2017,** *46*, 2520-2542.
(32) Rodríguez, L. M.; Gómez, P.; Más-Montoya, M.; Abad, J.; Tárraga, A.; Cerda, J. I.; Méndez, J.; Curiel, D.; Synthesis and two-dimensional chiral surface self-assembly of a π-conjugated system with three-fold symmetry: Benzotri(7-azaindole). *Angew. Chem. Int. Ed.* **2021,** *60*, 1782-1788.
(33) Jasper-Tönnies, T.; Gruber, M.; Ulrich, S.; Herges, R.; Berndt, R.; Coverage-controlled superstructures of C_3-symmetric molecules: Honeycomb versus hexagonal tiling. *Angew. Chem. Int. Ed.* **2020,** *59*, 7008-7017.
(34) Maeda, M.; Nakayama, R.; De Feyter, S.; Tobe, Y.; Tahara, K.; Hierarchical two-dimensional molecular assembly through dynamic combination of conformational states at the liquid/solid interface. *Chem. Sci.* **2020,** *11*, 9254-9261.
(35) Barth, J. V.; Costantini, G.; Kern, K.; Engineering atomic and molecular nanostructures at surfaces. *Nature* **2005,** *437*, 671-679.
(36) Urgel, J. I.; Di Giovannantonio, M.; Segawa, Y.; Ruffieux, P.; Scott, L. T.; Pignedoli, C. A.; Itami, K.; Fasel, R.; Negatively curved warped nanographene self-assembled on metal surfaces. *J. Am. Chem. Soc.* **2019,** *141*, 13158-13164.
(37) Dobscha, J. R.; Castillo, H. D.; Li, Y.; Fadler, R. E.; Taylor, R. D.; Brown, A. A.; Trainor, C. Q.; Tait, S. L.; Flood, A. H.; Sequence-defined macrocycles for understanding and controlling the build-up of hierarchical order in self-assembled 2D arrays. *J. Am. Chem. Soc.* **2019,** *141*, 17588-17600.
(38) Telychko, M.; Li, G. W.; Mutombo, P.; Soler-Polo, D.; Peng, X. N.; Su, J.; Song, S. T.; Koh, M. J.; Edmonds, M.; Jelínek, P.; Wu, J.; Lu, J.; Ultrahigh-yield on-surface synthesis and assembly of circumcoronene into a chiral electronic Kagome-honeycomb lattice. *Sci. Adv.* **2021,** *7*, eabf0269.
(39) Theobald, J. A.; Oxtoby, N. S.; Phillips, M. A.; Champness, N. R.; Beton, P. H.; Controlling molecular deposition and layer structure with supramolecular surface assemblies. *Nature* **2003,** *424*, 1029-1031.
(40) Korolkov, V. V.; Baldoni, M.; Watanabe, K.; Taniguchi, T.; Besley, E.; Beton, P. H.; Supramolecular heterostructures formed by sequential epitaxial deposition of two-dimensional hydrogen-bonded arrays. *Nat. Chem.* **2017,** *9*, 1191-1197.
(41) Gobbi, M.; Orgiu, E.; Samorì, P.; When 2D materials meet molecules: Opportunities and challenges of hybrid organic/inorganic van der waals heterostructures. *Adv. Mater.* **2018,** *30*, e1706103.
(42) Su, J.; Telychko, M.; Song, S.; Lu, J.; Triangulenes: From Precursor Design to On-Surface Synthesis and Characterization. *Angew. Chem. Int. Ed.* **2020,** *59*, 7658-7668.
(43) Wang, X.-Y.; Dienel, T.; Di Giovannantonio, M.; Barin, G. B.; Kharche, N.; Deniz, O.; Urgel, J. I.; Widmer, R.; Stolz, S.; De Lima, L. H.; Muntwiler, M.; Tommasini, M.; Meunier, V.; Ruffieux, P.; Feng, X.; Fasel, R.; Müllen, K.; Narita, A.; Heteroatom-doped perihexacene from a double helicene precursor: On-surface synthesis and properties. *J. Am. Chem. Soc.* **2017,** *139*, 4671-4674.
(44) Wang, X.-Y.; Urgel, J. I.; Barin, G. B.; Eimre, K.; Giovannantonio, M. D.; Milani, A.; Tommasini, M.; Pignedoli, C. A.; Ruffieux, P.; Feng, X.; Fasel, R.; Müllen, K.; Narita, A.; Bottom-up synthesis of heteroatom-doped chiral graphene nanoribbons. *J. Am. Chem. Soc.* **2018,** *140*, 9104-9107.

(45) During the preparation of this manuscript, Yang et al. deposited a preprint in ChemRxiv (on July 27th, 2022), describing the independent synthesis of OBO-doped [4]triangulenes with different substituents. See: Chen, X; Tan, D; Dong, J; Ma, T; Yang, D-T.; [4]Triangulenes with three oxygen-boron-oxygen (OBO) units and anti-kasha emissions. *ChemRxiv* **2022**, DOI: 10.26434/chemrxiv-2022-f0mfq.
(46) Wang, X.-Y.; Narita, A.; Zhang, W.; Feng, X.; Müllen, K.; Synthesis of stable nanographenes with OBO-doped zigzag edges based on tandem demethylation-electrophilic borylation. *J. Am. Chem. Soc.* **2016,** *138*, 9021-9024.
(47) Numano, M.; Nagami, N.; Nakatsuka, S.; Katayama, T.; Nakajima, K.; Tatsumi, S.; Yasuda, N.; Hatakeyama, T.; Synthesis of boronate-based benzo[fg]tetracene and benzo[hi]hexacene via demethylative direct borylation. *Chem. Eur. J* **2016,** *22*, 11574-11577.
(48) Galeotti, G.; De Marchi, F.; Taerum, T.; Besteiro, L. V.; El Garah, M.; Lipton-Duffin, J.; Ebrahimi, M.; Perepichka, D. F.; Rosei, F.; Surface-mediated assembly, polymerization and degradation of thiophene-based monomers. *Chem. Sci.* **2019,** *10*, 5167-5175.
(49) Galeotti, G.; De Marchi, F.; Hamzehpoor, E.; MacLean, O.; Rajeswara Rao, M.; Chen, Y.; Besteiro, L. V.; Dettmann, D.; Ferrari, L.; Frezza, F.; Sheverdyaeva, P. M.; Liu, R.; Kundu, A. K.; Moras, P.; Ebrahimi, M.; Gallagher, M. C.; Rosei, F.; Perepichka, D. F.; Contini, G.; Synthesis of mesoscale ordered two-dimensional π-conjugated polymers with semiconducting properties. *Nat. Mater.* **2020,** *19*, 874-880.
(50) Lu, J.; Jiang, H.; Yan, Y.; Zhu, Z.; Zheng, F.; Sun, Q.; High-throughput preparation of supramolecular nanostructures on metal surfaces. *ACS Nano* **2022**, DOI: 10.1021/acsnano.1022c06294.